processes

MDPI

Article

Numerical Simulations of Gasification of Low-Grade Coal and Lignocellulosic Biomasses in Two-Stage Multi-Opposite Burner Gasifier

Anees u Rehman [1], Imran Nazir Unar [1,*], Masroor Abro [1], Khadija Qureshi [1], Sikandar Almani [1] and Abdul Sattar Jatoi [2]

1 Process Simulation and Modeling (PSM) Research Group, Department of Chemical Engineering, Mehran University of Engineering and Technology, Jamshoro 76062, Pakistan; aneesrehman43@quest.edu.pk (A.u.R.); masroor.abro@faculty.muet.edu.pk (M.A.); khadija.qureshi@faculty.muet.edu.pk (K.Q.); sikander.almani@faculty.muet.edu.pk (S.A.)

2 Department of Chemical Engineering, Dawood University of Engineering & Technology, Karachi 74800, Pakistan; abdul.sattar@duet.edu.pk

* Correspondence: imran.nazir@faculty.muet.edu.pk; Tel.: +92-333-3314744

Abstract: Thermochemical processes utilizing biomass demonstrate promising prospects for the generation of syngas. In this work, a gasification process employing combination of an indigenous low-grade coal with two distinct biomass sources, namely rice husk (RH) and wood sawdust (WS), was explored. The gasification of the selected feedstock was performed using a double-staged multi-opposite burner (MOB) gasifier. A 3D computational fluid dynamics (CFD) model was employed to analyze the effect of kinetic and diffusion rates on the overall gasification performance of an entrained flow biomass gasifier. DPM was employed to track the particles' trajectory, while the gas phase was treated as the continuous phase, and its behavior was predicted using a standard k-epsilon turbulent model. To calculate both the homogeneous and heterogeneous reaction rates, the finite rate/eddy dissipation model was implemented. The findings indicate that the char conversion efficiency exceeded 95% across all instances. Among the different reaction schemes, scheme E (which involved complete volatile and char combustion reactions) produced better results in comparison with published results, with less than 1% error. Hence, scheme E was validated and utilized for the rest of the simulated cases. The feeding rate has an inverse effect on the overall performance of the gasifier. An increase in feed rate decreases the CO and H_2 composition in syngas. The maximum CO value was observed to be 57.59% at a 1.0 O/C ratio with a 0.005 kg/s feed rate, and the maximum H_2 value was observed to be 16.58% in the same conditions for Lakhra coal samples. In summary, Lakhra coal exhibited better performance than other biomass samples due to its better fixed carbon and volatiles in its composition.

Keywords: biomass gasification; multi-opposite burner gasifier; lignocellulosic biomasses

check for updates

Citation: Rehman, A.u.; Unar, I.N.; Abro, M.; Qureshi, K.; Almani, S.; Jatoi, A.S. Numerical Simulations of Gasification of Low-Grade Coal and Lignocellulosic Biomasses in Two-Stage Multi-Opposite Burner Gasifier. *Processes* **2023**, *11*, 3451. https://doi.org/10.3390/pr11123451

Academic Editor: Yu-Cai He

Received: 6 November 2023
Revised: 27 November 2023
Accepted: 3 December 2023
Published: 18 December 2023

Copyright: © 2023 by the authors. Licensee MDPI, Basel, Switzerland. This article is an open access article distributed under the terms and conditions of the Creative Commons Attribution (CC BY) license (https://creativecommons.org/licenses/by/4.0/).

1. Introduction

Nonrenewable energy has been a major source of primary energy in the world for the last few decades. It has been reported in the past literature that oil and natural gas resources will be consumed in the forthcoming 40 to 50 years [1]. On the other hand, coal reserves have great potential and longevity, exceeding 100 years, to satisfy energy needs. Consequently, the application of coal as a substitute for oil and natural gas is becoming increasingly popular. In contrast, the application of coal for energy production over the past many decades has caused several serious environmental and hygienic problems such as emissions of carbon dioxide, SO_x, and NO_x. Owing to these problems, though coal is used for energy generation, it has become extremely important to develop a method to utilize coal in a cleaner way.

Biomass is a significant source of renewable energy, providing 10% of the primary-energy demand in the world, according to International Energy Agency (IEA) reports in 2011. Various materials such as municipal solid waste, agricultural waste, petroleum coke, forest waste, and wood waste can serve as viable feedstocks in the process of gasification [2–4]. Looking forward, biomass is suggested to satisfy half of the global energy demand [5,6]. The direct combustion of biomass for energy production is not appropriate. The drawbacks associated with the direct combustion of biomass include a low heating value, which is inappropriate for its high-temperature application as a fuel, so the direct combustion of biomass in internal combustion engines is not possible [7]. Co-gasification of coal with biomass is a promising way to generate cleaner energy and presently, it is being adopted by different countries [8–10]. The main components of producer gas obtained through the gasification of coal and biomass are CO and H_2 [11,12]. Considering the industrial demands for fuel, raw biomasses undergo conversion via biochemical, thermochemical, and extraction methodologies to yield a more adaptable fuel [13,14]. The syngas produced through thermochemical conversion processes is a more versatile fuel than the original raw material used for numerous applications such as electricity production, H_2 production, and heat generation [15].

Syngas quality is notably affected by various factors including the design of the gasifier and the properties of the fuel such as particle size, moisture content, operating conditions such as gasification temperature, equivalence ratio, pressure, and the gasifying medium [15–17]. Compared to coal, raw biomass contains a low energy density and a high moisture content. Therefore, a deep understanding of all chemical and physical changes occurring in biomass is important for the successful and efficient operation of biomass gasification plants. To this end, numerical methods provide a dependable means to understand the effect of varying gasifier operating conditions such as pressure and temperature and reaction kinetics. For the simulation and visualization of the gasification processes, the CFD tool has remained an effective tool over the last 20 years [18–22]. Various numerical models have been used for the prediction of gasification phenomena; for example, the Euler–Euler model has been applied for the prediction of solid and gas behavior inside a reactor [23–25], while some researchers have used the Euler–Lagrangian model to study solid and gas relations [26,27]. Finite rate/eddy dissipation models and the probability density functions (PDF) model are frequently applied to investigate the kinetics of gasification reactions. CFD simulations have been successfully used to investigate the effects of major design and operating parameters on gasification reactions [19,28–30].

Three configurations of gasifiers, i.e., fixed bed, fluidized bed, and entrained flow gasifiers, have been used for gasification. Each configuration has its characteristic features; however, the entrained flow gasifier (EFG) can preferably be used in an integrated gasification combined cycle (IGCC) because of the short residence time and high carbon conversion efficiencies [31,32]. EFGs with multi-opposite burners (MOBs) are gaining prominence in scientific research due to their characteristics of greater collision rates between solid particles and better fuel conversion efficiencies [33,34]. Until now, both experimental and simulation-based methods have been used to optimize their design. Scaled-down methods are usually used for optimization of gasifier geometry through experimental investigations. However, the experiment-based approach is costly and time-consuming, with many limitations to gaining a deep understanding of gasification for geometry optimization. Moreover, the data obtained in the scaled-down method may not fully extrapolate to a pilot scale. Hence, different researchers prefer using computer-based methods to investigate gasification processes [6,35–37]. Computer-aided simulations can provide a huge data pool for measuring different operating parameters over a broad range. Computational fluid dynamics (CFD) is a commonly used modeling tool in numerous engineering applications [26,38–40]. In the context of gasification, CFD simulations can be performed for wide ranges of particle size, feed properties, moisture content, and O/C ratio and superficial velocity, etc., as well as for the optimization of gasifier geometry.

In the current research scenario, there is significant emphasis on double-staged entrained flow gasifiers with multi opposite burners (MOBs), as these are recognized for their excellent performance owing to the vigorous mixing of feedstock and the oxidizing agent [32]. MOB gasifiers are sensitive to feed conditions and have never been tested for biomass gasification with impinging and tangential nozzles at two stages. The O/C ratio and coal feeding are an important parameter for gasification and hence need an investigation regarding their impact on biomass gasification in a MOB gasifier. Hence, the aim of current study was to examine the gasification process combining Pakistani coal from the Lakhra field and different biomass samples, with varying oxygen-to-fuel ratios, and to assess its impact on syngas quality, including gas composition and carbon conversion efficiency.

2. Numerical Method

2.1. CFD Model Development

The computational domain of the MOB gasifier was developed; subsequently, governing equations were selected to understand the gasification phenomena.

2.2. Computational Domain

The entrained flow gasifier as described by Ambatipudi and Varunkumar [41] was used in this study with slight modification as shown in Figure 1. The dimensional specifications of the gasifier are given in Table 1. In their study, a horizontal flow configuration was used, whereas the current study employed a vertical flow gasifier design. The meshed structure of the gasifier is illustrated in Figure 2. The geometry was developed in Ansys Design Modeler®19.1 and the meshing was performed in Ansys Meshing®19.1. The gasifier consisted of two nozzles on each level with central and tangential orientation. Biomass/coal as a feedstock was injected from the central nozzles, whereas oxygen as a gasifying medium was injected through tangential nozzles. Initially, meshes of four different sizes were developed; the details are presented in Table 2. The mesh independence test was performed by comparing the temperature profile along the central axis for all mesh sizes as shown in Figure 3. It has been observed that finer and finest meshes show almost similar temperature results. Hence, the finer mesh was considered the optimized mesh and beyond this density of grid, the solution become independent of the result.

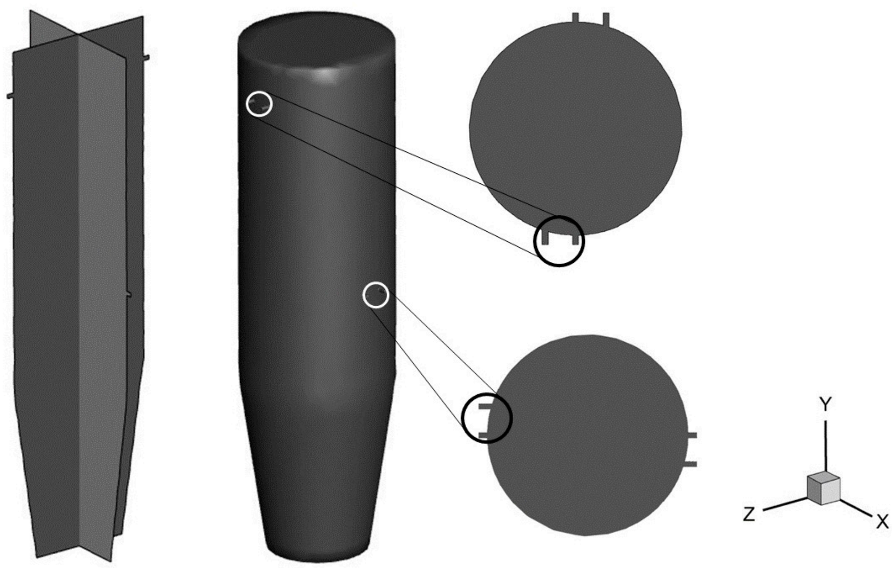

Figure 1. Different views of 3D computational domain of MOB gasifier.

Table 1. The dimensions of geometry.

Sr. No	Specification	Value
1	Diameter of main gasifier body	350 mm
2	Height	1200 mm
3	Diameter of inlet nozzles	10 mm
4	Outlet diameter	230 mm

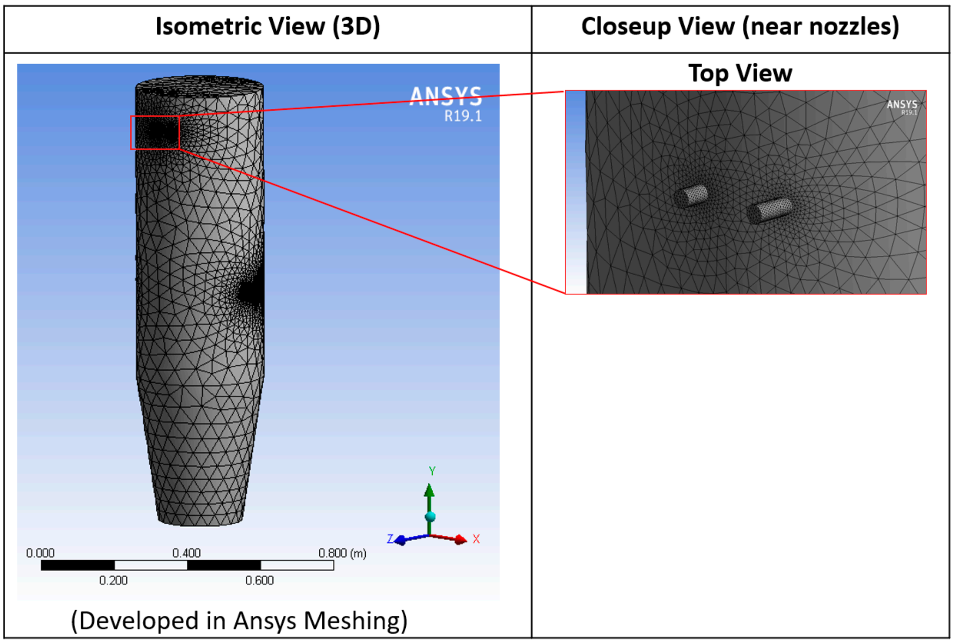

Figure 2. Meshed geometry with closed view of nozzles.

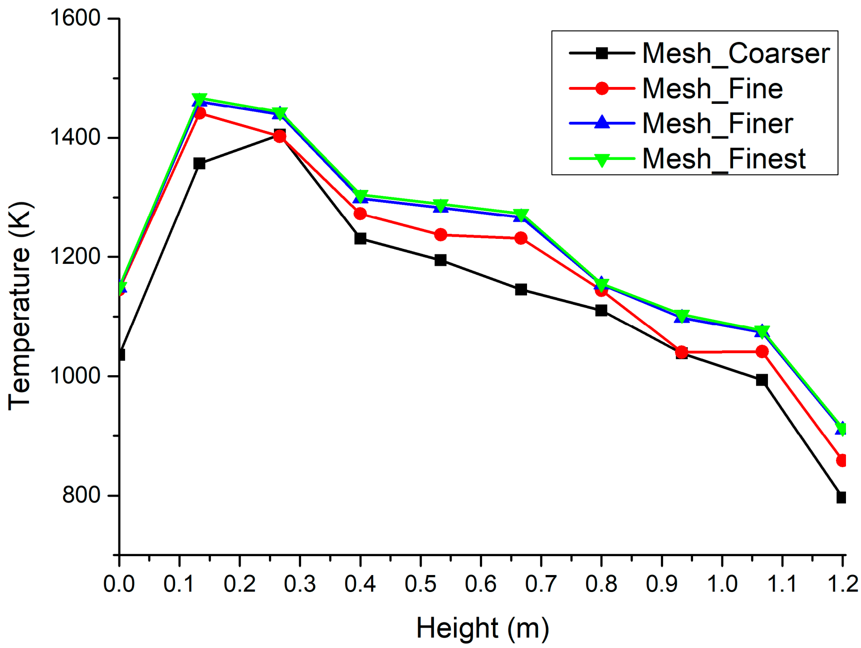

Figure 3. Temperature profile along central axis with different grids.

Table 2. Different meshes with varying quantity of elements.

Sr. No	Grid Name	No. of Elements
1	Coarser mesh	78,457
2	Fine mesh	89,748
3	Finer mesh	112,185
4	Finest mesh	185,850

2.3. Governing Equations and Assumptions

The processes taking place in the gasifier, i.e., mass transfer, heat transfer, and the chemical reactions of homogeneous and heterogeneous nature were captured by converging the governing equations described in Table 3. Some assumptions were made in a numerical setting: (1) An incompressible, turbulent, axisymmetric, and steady-flow field was assumed; (2) the formation of the air pollutants COS, CS_2, HCN, NH_3, and H_2S during gasification process were ignored. (3) The body force of the flow and the thermal radiation in the reactor were omitted. (4) The gasifier wall was deemed adiabatic. The Navier–Stokes equations coupled with the energy and species equations in both steady-state and time-averaged forms were resolved alongside the conventional k-epsilon turbulence model. Detailed information about the governing equations and their associated constants is provided in Table 3, following the strategies of previous research [42–44].

Table 3. List of governing equations.

Physics	Governing Equations	Equation No.
Continuity	$\frac{\partial}{\partial x_i}\left(\rho u_{ij}\right) = \frac{\Delta m_p}{m_{p,0}}\, \dot{m}_{p,0}$	(1)
Momentum	$\frac{\partial}{\partial x_i}\left(\rho u_i u_j\right) = -\frac{\partial p}{\partial x_j} + \frac{\partial}{\partial x_i}\left(\tau_{ij} - \overline{\rho u'_i u'_j}\right) + \sum\left[\frac{18\mu C_D Re}{\rho_p d_p^2 24}\left(u_p - u\right)\right]\dot{m}_p \Delta t$	(2)
Energy	$\frac{\partial}{\partial x_i}\left(\rho c_p u_i T\right) = \frac{\partial}{\partial x_i}\left(\lambda\frac{\partial T}{\partial x_i} - \rho c_p \overline{u'_i T'}\right) - \sum_j \frac{\Delta H_j^0}{M_j}\overline{R_j}$	(3)
Species transport model	$\frac{\partial}{\partial x_i}\left(\rho c_p u_i T\right) = \frac{\partial}{\partial x_i}\left(\lambda\frac{\partial T}{\partial x_i} - \rho c_p \overline{u'_i T'}\right) - \sum_j \frac{\Delta H_j^0}{M_j}\overline{R_j}$	(4)
Kinematic viscosity	$\mu_t = \rho C_\mu k^2/\varepsilon$	(5)
Kinetic energy	$\frac{\partial}{\partial x_i}\left(\rho u_i k\right) = \frac{\partial}{\partial x_i}\left[\left(\mu + \frac{\mu_t}{\sigma_k}\right)\frac{\partial k}{\partial x_i}\right] + G_k - \rho\varepsilon$	(6)
Dissipation rate	$\frac{\partial}{\partial x_i}\left(\rho u_i k\right) = \frac{\partial}{\partial x_i}\left[\left(\mu + \frac{\mu_t}{\sigma_k}\right)\frac{\partial k}{\partial x_i}\right] + G_k - \rho\varepsilon$	(7)
Heat conductivity	$\rho c_p \overline{u'_i T'} = -\lambda\frac{\partial T}{\partial x_i} = -C_p \frac{\mu_t}{Pr_t}\frac{\partial T}{\partial x_i}$	(8)
Diffusion coefficient	$\rho u'_i \overline{Y'}_j = -\rho D\frac{\partial Y}{\partial x_i} = -\frac{\mu_t}{SC_t}\frac{\partial Y}{\partial x_i}$	(9)
Discrete phase model		
Change in velocity of a particle	$Fd = \frac{m_p dV_P}{dt}$	(10)
Drag force	$F_D = \frac{\rho A_{p,c} C_D v_r^2}{2}$	(11)
Constants	$C_\mu = 0.09$ $C_{1\epsilon} = 1.44$ $C_{2\epsilon} = 1.92$ $\sigma_k = 1.0$ $\sigma_\epsilon = 1.3$ $Pr_t = 0.85$ $Sc_t = 0.7$	

2.4. Chemical Reactions

The decomposition of feed particles into volatiles, char, and ash at higher temperatures may be given as [45]:

$$Fuel \rightarrow \alpha_1 CH_4 + \alpha_2 H_2 + \alpha_3 CO + \alpha_4 CO_2 + \alpha_5 H_2O + \alpha_6 Char + \alpha_7 Ash \sum_i \alpha i = 1 \quad (12)$$

At the initial material feeding stage, the devolatilization process of the raw material dominates over the other process [46]. Within the devolatilization process, the release of volatiles occurs through a two-step devolatilization mechanism [47]. The two-step devolatilization model can be written as:

The devolatilization at low temperature is represented as

$$Fuel \xrightarrow{k_l} (1 - Y_l) \times Char_l + Y_l \times volatile \quad (13)$$

whereas the devolatilization at high temperature is written as

$$Fuel \xrightarrow{k_h} (1 - Y_h) \times Char_h + Y_h \times volatile \quad (14)$$

Y stands for the stoichiometric coefficient. Equation (13) governs reactions at lower temperatures, whereas Equation (14) takes precedence at higher temperatures. Consequently, the reaction kinetics for volatiles can be described as follows:

$$\frac{dV}{dt} = (k_l Y_l + k_h Y_h) Fuel \quad (15)$$

$$k_l = A_l exp\left(-\frac{E_{a,l}}{RT_p}\right) \quad (16)$$

$$k_h = A_h exp\left(-E_{a,h}/RT_p\right) \quad (17)$$

T_P signifies the temperature of the feed particles, V represents the fraction of mass consisting of volatiles, A corresponds to the pre-exponential factor, k denotes the reaction rate constant, and Ea signifies the activation energy for the reactions. The E_h, E_l, Y_h, Y_l, K_h, and K_l values are given in Table 4 [32,47].

Table 4. Kinetic parameters for devolatization process.

Parameter	Value
K_h s^{-1}	1.28×10^7
K_l s^{-1}	200,000
Y_h	1
Y_l	0.29
E_h $\left(\text{KJmol}^{-1}\right)$	165.3
E_l $\left(\text{KJmol}^{-1}\right)$	106.9

Char produced from coal devolatilization results in the formation of CO and H_2 during its gasification. Different researchers have selected various reactions to define the gasification reaction mechanism [32,48–50]. The gasification process starts with the breakup of feedstock into different species as per Equation (10). Later, several homogeneous and heterogeneous reactions occur due to the availability of appropriate species and thermodynamic conditions. Table 5 describes all these reactions along with their kinetic information. In this work, preliminary simulations were carried out with different reaction plans (from A to F per Table 3) to find the best reaction plan based on the comparison with previous experimental research conducted by Ambatipudi and Varunkumar [41].

Table 5. Various reaction mechanisms with their kinetic data [32,48].

Sr. No	Reactions	Schemes						Kinetic Parameters	
		A	B	C	D	E	F	A (Pre-Exponent Factor)	E (Activation Energy)
Homogeneous Reactions									
1 *	Vol + X O_2 → A CO_2 + B H_2O + C N2 + D SO_2 (Volatiles complete combustion)							2.119×10^{11}	2.03×10^{8}
2 *	Vol + X′ O_2 → A′ CO + B H_2O + C N2 + D SO_2 (Volatiles partial combustion)							2.12×10^{11}	2.20×10^{11}
3	$CO + 0.5O_2 \rightarrow CO_2$ $\Delta H^0 = -283$ MJkmol^{-1} (CO combustion)							2.239×10^{12}	1.70×10^{8}
4	$H_2 + 0.5O_2 \rightarrow H_2O$ $\Delta H^0 = -242$ MJkmol^{-1} (H_2 combustion)							6.800×10^{15}	1.68×10^{8}
5	$CO + H_2O \rightarrow CO_2 + H_2$ $\Delta H^0 = -41.1$ MJkmol^{-1} (Water shift reaction) (f)							2.750×10^{10}	8.38×10^{7}
6	$CO_2 + H_2 \rightarrow CO + H_2O$ $\Delta H^0 = 41.1$ MJkmol^{-1} (Water shift reaction) (b)							0.0265	3960
Heterogeneous Reactions									
7	$C + \frac{1}{2}O_2 \rightarrow CO$ $\Delta H^0 = -111$ MJkmol^{-1} (Char partial combustion)							0.052	6.10×10^{7}
8	$C + O_2 \rightarrow CO_2$ $\Delta H^0 = -393$ MJkmol^{-1} (Char complete combustion)							415.7	9.04×10^{7}
9	$C + CO_2 \rightarrow 2CO$ $\Delta H^0 = +111$ MJkmol^{-1} (Gasification, Boudourad reaction)							107,800	2.44×10^{7}
10	$C + H_2O \rightarrow CO + H_2$ $\Delta H^0 = +131$ MJkmol^{-1} (Gasification)							97,540	2.02×10^{8}

* Reactions 1 and 2 are dependent on the feed composition.

Regarding species equations, Sr represents the sum of reaction rates of different species and is written as:

$$S_r = \sum_{j=1}^{Nr} M_{j,r} W_{j,r} \tag{18}$$

$$W_{j,r} = \left(v''_{j,r} - v'_{j,r}\right) k_f \left(\prod_{i=1}^{Nr} C_i^{n'} - \frac{1}{K_{eq}} \prod_{i=1}^{Nr} C_i^{n''}\right) \tag{19}$$

$$k_f = AT^B e^{-Ea/RT} \tag{20}$$

The forward reaction rate constant, k_f, in the equation above was derived according to the Arrhenius law. In this context, 'A' represents the pre-exponential factor, while 'E' signifies the activation energy. Detailed values for 'A' and 'E' pertaining to various reactions can be found in Table 5.

2.5. Feedstock Composition, Operating Parameters, and Performance Indicators

The feedstocks used in the gasifier include LC, RH, and WS. The proximate and ultimate analysis of all the feedstock samples were conducted in the Hi-Tech laboratory of Jamshoro. The composition obtained from experiments is tabulated in Table 6.

The stoichiometric reactions of fuels with oxygen could be written as:

Wood sawdust:

Complete

$$C_{0.82}H_{2.12}O_{1.11}N_{0.0092}S_{0.0021} + 0.80O_2 \rightarrow 0.82CO_2 + 1.06H_2O + 0.0046N_2 + 0.0021SO_2 \tag{21}$$

Partial

$$C_{0.82}H_{2.12}O_{1.11}N_{0.0092}S_{0.0021} + 0.38O_2 \rightarrow 0.82CO_2 + 1.06H_2O + 0.0046N_2 + 0.0021SO_2 \tag{22}$$

Rice husk:

Complete

$$C_{0.80}H_{2.22}O_{1.12}N_{0.008} + 0.8O_2 \rightarrow 0.80CO_2 + 1.11H_2O + 0.004N_2 \quad (23)$$

Partial

$$C_{0.80}H_{2.22}O_{1.12}N_{0.008} + 0.4O_2 \rightarrow 0.80CO_2 + 1.11H_2O + 0.004N_2 \quad (24)$$

Lakhra coal:
Complete

$$C_{1.1}H_{4.07}O_{0.44}N_{0.053}S_{0.1461} + 2.04O_2 \rightarrow 1.10CO_2 + 2.03H_2O + 0.0265N_2 + 0.1461SO_2 \quad (25)$$

Partial

$$C_{1.1}H_{4.07}O_{0.44}N_{0.053}S_{0.1461} + 1.49O_2 \rightarrow 1.10CO + 2.03H_2O + 0.0265N_2 + 0.1461SO_2 \quad (26)$$

For the evaluation of the performance of a gasification plant, carbon conversion efficiency and cold gas efficiency are two important parameter indices and can be represented by the following equations [51].

$$CC(\%) = \left(1 - \frac{m_{out}\left(y_{CO_2}\frac{12}{44} + y_{CO}\frac{12}{28}\right)}{m_{in,fuel}y_c}\right) \times 100 \quad (27)$$

$$CGE(\%) = \frac{m_{out}\left(y_{H_2}HHV_{H_2} + y_{CO}HHV_{CO}\right)}{m_{in,fuel}HHV_{fuel}} \times 100 \quad (28)$$

The carbon conversion efficiency was determined by investigating CO and CO_2 concentrations, while the cold gas efficiency was ascertained by examining the levels of H_2 and CO concentrations.

Table 6. Proximate, ultimate, and calorific analysis results of selected feedstocks.

Biomass Type	Lakhra Coal	Rice Husk	Wood Sawdust
Proximate analysis (wt.%, dry basis)			
M	9.93	4.83	5.53
VM	43.69	61.86	72.60
FC	31.96	15.30	14.55
Ash	14.42	18.01	7.32
Ultimate analysis (wt. %, dry basis)			
C	67.84	45.8	44.1
H	7.9	6	5.96
N	1.43	0.3	0.36
O	13.81	47.9	49.39
S	9.02	0	0.19
HHV (J kg^{-1})	1.89×10^7	1.33×10^7	1.88×10^7

2.6. Conditions at Boundary Zones and Solution Strategies

The feedstock, initially at 300 K, was introduced through the central nozzles of both level injectors, while oxygen was supplied via the tangential injectors at both levels. The feed particle size was controlled within the range of 56 to 250 μm, with an observed average particle size of 113 μm. The feed particle size was controlled within the range of 56 to 250 μm, with an observed average particle size of 113 μm. The sizing of the feed particles was assessed using the Rosin–Rammler distribution function [52]. Due to the reactor's axisymmetric centerline design, there was a restriction preventing mass and heat fluxes from crossing the system boundaries. Additionally, no-slip conditions were applied, considering the reactor's adiabatic wall. The numerical investigation of biomass gasification phenomena was conducted using ANSYS FLUENT® 19.0 software. The SIMPLE algorithm was employed to solve the governing equations and manage the boundary conditions within these simulations. Meanwhile, for the calculation of diffusion fluxes and convection, a first-order upwind scheme was utilized. The feedstock type, feedstock flowrate (feeding rate) and O/C ratio were the varying parameters. Total 27 cases were simulated, whose parametric information is given in Table 7. A Core i7 PC with 1.30 GHz and 1.50 GHz processing speed was used, having 16 GB RAM along with a 4 GB graphics card. Each simulation took about 3 to 4 h to be solved.

Table 7. Input conditions for the simulated cases.

Sr. No	Case Name	Feedstock	Feeding Rate (kg/s)	O/C Ratio	Oxidant Flowrate (kg/s)	Oxidant Distribution (kg/s)	
						Up-Nozzles (60%)	Down-Nozzles (40%)
1	LC_0.005_0.9	LC	0.005	0.9	0.0024	0.00072	0.00048
2	LC_0.005_1.0	LC	0.005	1.0	0.0027	0.00081	0.00054
3	LC_0.005_1.1	LC	0.005	1.1	0.003	0.0009	0.0006
4	LC_0.01_0.9	LC	0.01	0.9	0.0047	0.00141	0.00094
5	LC_0.01_1.0	LC	0.01	1.0	0.0054	0.00162	0.00108
6	LC_0.01_1.1	LC	0.01	1.1	0.0061	0.00183	0.00122
7	LC_0.015_0.9	LC	0.015	0.9	0.0071	0.00213	0.00142
8	LC_0.015_1.0	LC	0.015	1.0	0.0081	0.00243	0.00162
9	LC_0.015_1.1	LC	0.015	1.1	0.0091	0.00273	0.00182
10	RH_0.005_0.9	RH	0.005	0.9	0.0206	0.00618	0.00412
11	RH_0.005_1.0	RH	0.005	1.0	0.0229	0.00687	0.00458
12	RH_0.005_1.1	RH	0.005	1.1	0.0252	0.00756	0.00504
13	RH_0.01_0.9	RH	0.01	0.9	0.0041	0.00123	0.00082
14	RH_0.01_1.0	RH	0.01	1.0	0.0458	0.01374	0.00916
15	RH_0.01_1.1	RH	0.01	1.1	0.0504	0.01512	0.01008
16	RH_0.015_0.9	RH	0.015	0.9	0.0618	0.01854	0.01236
17	RH_0.015_1.0	RH	0.015	1.0	0.0687	0.02061	0.01374
18	RH_0.015_1.1	RH	0.015	1.1	0.0756	0.02268	0.01512
19	WS_0.005_0.9	WS	0.005	0.9	0.002	0.0006	0.0004
20	WS_0.005_1.0	WS	0.005	1.0	0.0022	0.00066	0.00044
21	WS_0.005_1.1	WS	0.005	1.1	0.0024	0.00072	0.00048
22	WS_0.01_0.9	WS	0.01	0.9	0.004	0.0012	0.0008
23	WS_0.01_1.0	WS	0.01	1.0	0.0044	0.00132	0.00088
24	WS_0.01_1.1	WS	0.01	1.1	0.0049	0.00147	0.00098
25	WS_0.015_0.9	WS	0.015	0.9	0.006	0.0018	0.0012
26	WS_0.015_1.0	WS	0.015	1.0	0.0066	0.00198	0.00132
27	WS_0.015_1.1	WS	0.015	1.1	0.0073	0.00219	0.00146

The convergence criteria for mass, momentum, and specie equations were set at 0.0001, whereas for energy and the P-1 radiation model, the convergence criteria were set at

1×10^{-6}. The energy and P-1 radiation equations are most the sensitive in terms of solving for gasification cases.

3. Results and Discussion

Biomass wastes including RH and SD along with Lakhra coal were selected for this study. The proximate analysis, ultimate analysis, and higher heating values of all selected biomasses are summarized in Table 6. In this work, the O/C ratio was maintained from 0.9 to 1.1 by changing the mass flow rate of feedstock.

3.1. Validation of Reaction Schemes

Prior to the parametric investigation, the modeling strategy, particularly the reaction schemes, were validated through experimental research work conducted by Ambatipudi and Varunkumar [38]. For the validation purpose, the same feedstocks, i.e., coal and groundnut shells, were used by taking the composition cited in the mentioned research work. The feeding rate for coal and groundnut were maintained at 5.4 and 8.0 kg/h, respectively. The composition for oxidizing gas for coal and groundnut shell gasification were maintained at 30% O_2–48% CO_2 and 23% O_2–59% CO_2, respectively. The estimated mole fractions of the important components (CO, H_2 and CO_2) of simulated syngas with different reaction schemes are compared with experimental data [38] in Figure 4a,b for the gasification of coal and groundnut shell feedstocks, respectively.

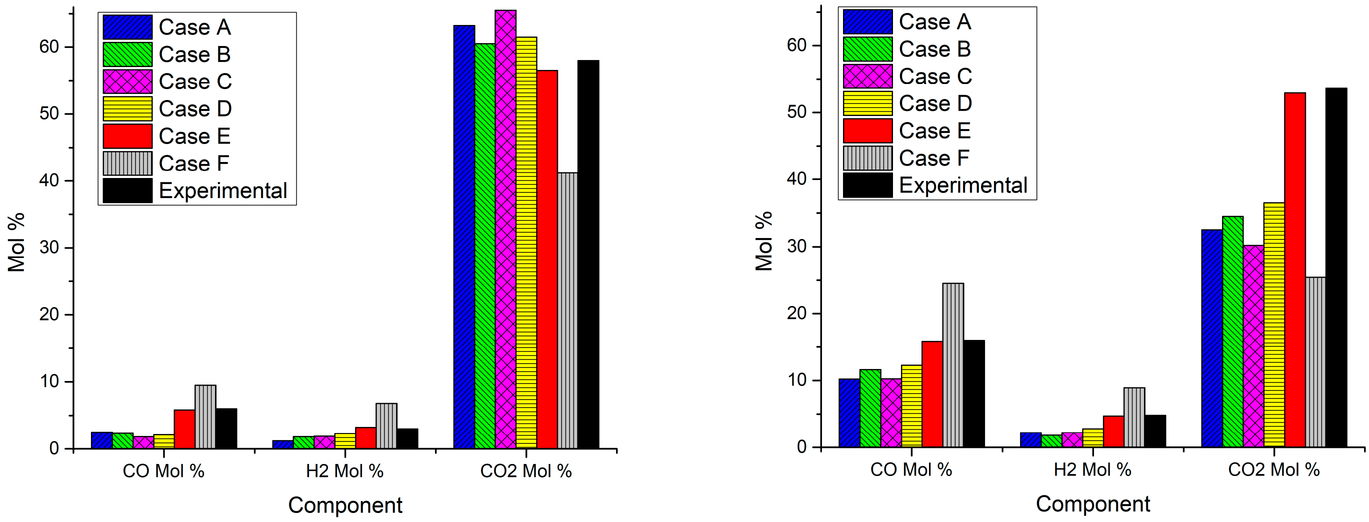

(**a**) Coal (**b**) Groundnut shells

Figure 4. Mole fraction of important components of syngas from the gasification of various feedstocks at different reaction schemes.

The results suggest that reaction scheme E estimated the mole fractions of CO, H_2, and CO_2 with the error in the range of 1–5% using both feedstocks; it was observed that scheme E predicted the results well, per previous research [32,44]. Therefore, the rest of the simulations were performed by taking scheme E as the base reaction scheme.

3.2. Syngas Composition

The produced syngas is usually evaluated via its composition. Among various species, CO, H_2, and CO_2 have primary importance in gasification. Following the trends of previous researchers, the CO, H_2, and CO_2 mole fractions were estimated from all the cases. Their compositions were plotted against an O/C ratio at different feed rates for LC, RH and WS in Figure 5a–c respectively. It was observed that CO and H_2 showed their maximum values at O/C ratio = 1.0, which is consistent to the trend obtained in previous studies [32,53]. After 1.0, the combustion scenario dominated, as observed by the increasing CO_2 concentration.

The maximum mole fractions of CO were observed to be 57.59%, 36.57%, and 47.54% for the LC, RH, and WS feedstocks, respectively. Similarly, the maximum mole fractions of H_2 were observed to be 16.58%, 23.54%, and 13.47% for the LC, RH, and WS feedstocks, respectively. It was seen that higher CO mole fraction values were achieved with coal as feedstock as compared to biomass feedstocks due to higher fixed carbon in coal. On the other hands, the higher H_2 mole fraction was achieved with biomass feedstocks as compared to coal due to higher amount of moisture in biomass samples.

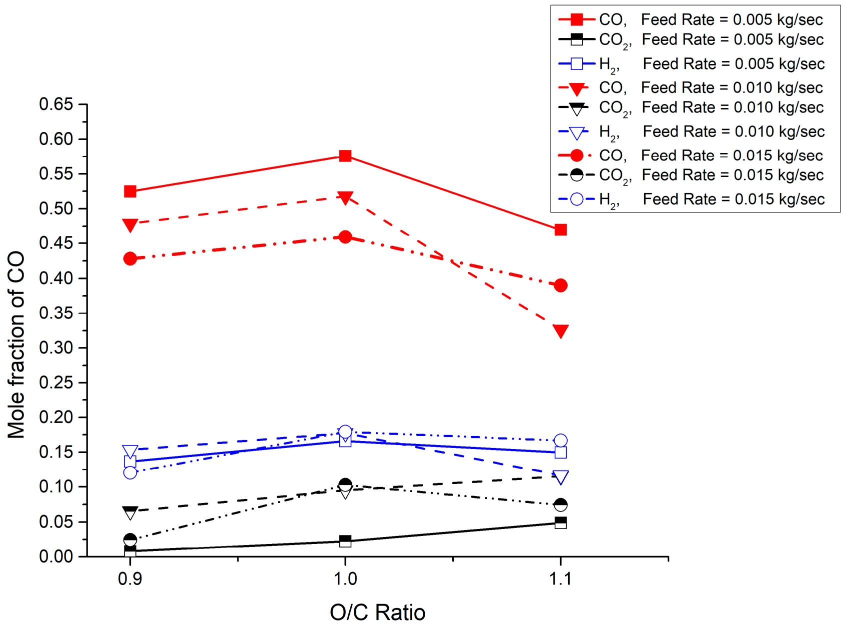

(**a**) Lakhra Coal

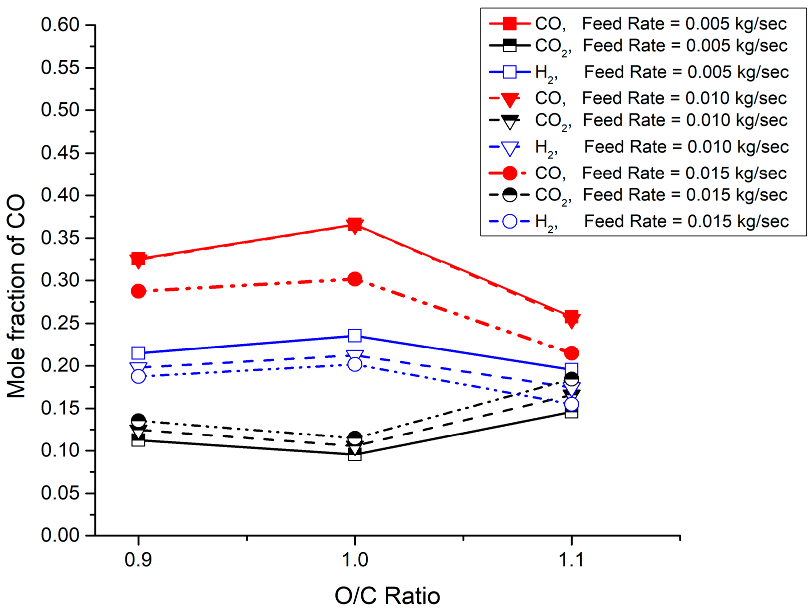

(**b**) Rice Husk

Figure 5. *Cont.*

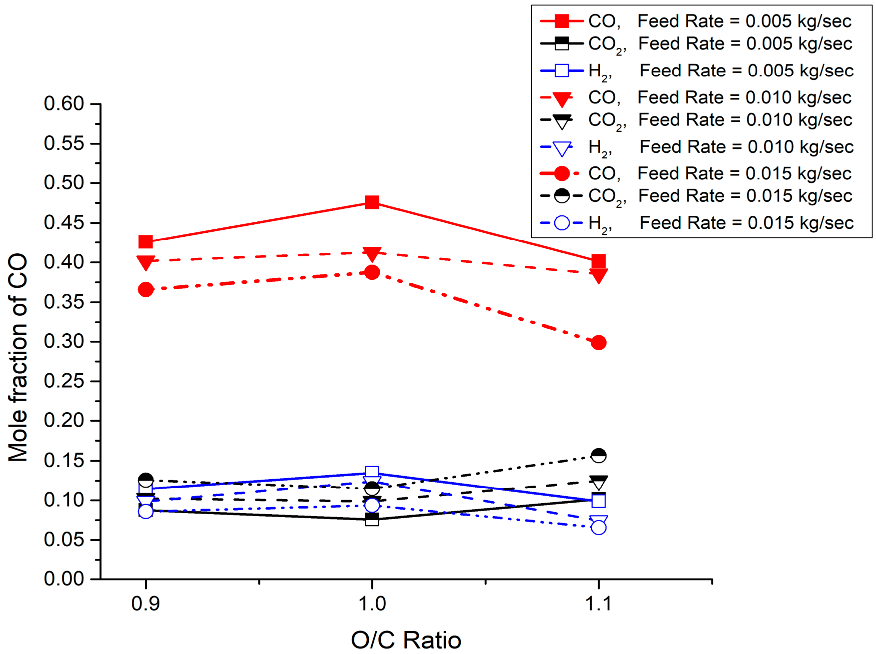

(**c**) Wood Sawdust

Figure 5. Syngas composition at varying O/C ratios and feedstock feeding rate with Lakhra coal as feedstock.

The production trends of CO, CO_2, and H_2 are illustrated by mole fraction profiles in Figure 6a–c for selected feedstocks. The findings suggest that combustion prevails in the upper region of the gasifier due to higher amounts of CO_2 production. However, near the gasifier bottom, the gasification reactions play their role, exhibiting higher conversion of CO and H_2.

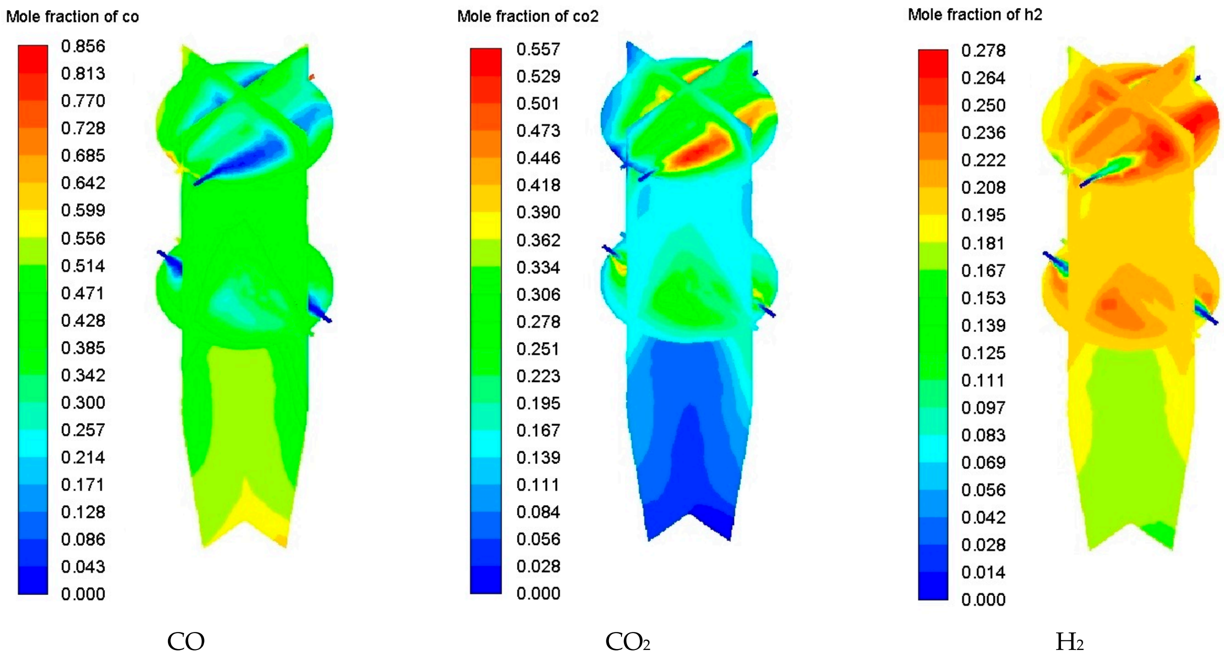

(**a**) Lakhra Coal

Figure 6. *Cont.*

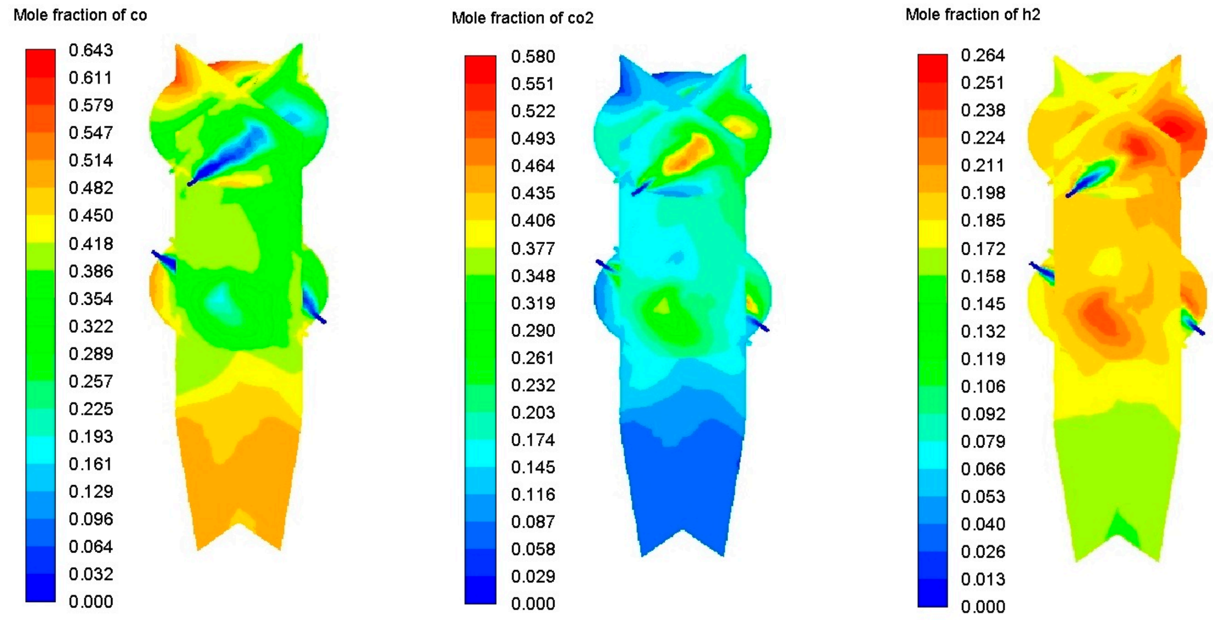

CO CO$_2$ H$_2$

(**b**) Rice Husk

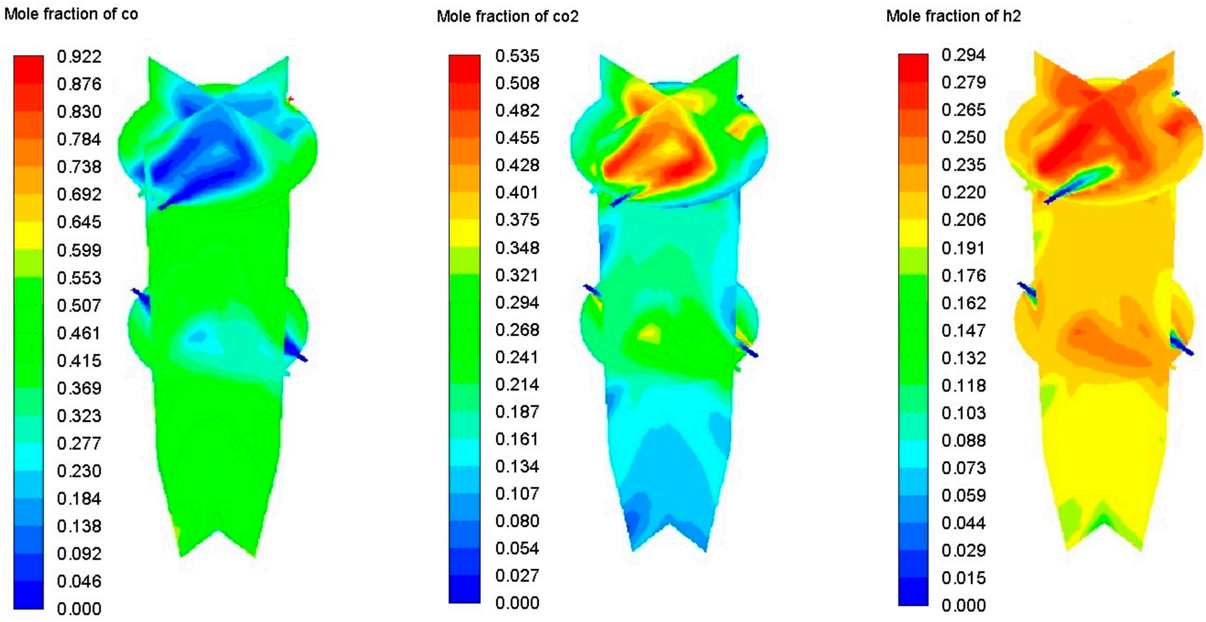

CO CO$_2$ H$_2$

(**c**) Wood Sawdust

Figure 6. Contours of CO, CO_2, and H_2 mole fraction produced from WS at optimized conditions.

3.3. Temperature of Gasification

Study of the temperature profiles within the chamber of the gasifier is crucial for evaluating its performance. Therefore, the temperature of syngas produced in each scenario is compared in Figure 7a–c. The maximum temperatures of syngas produced from all the selected feedstocks were achieved at higher O/C ratio and higher feeding rate, i.e., 1.1 and 0.015 kg/s respectively. This could be attributed to the dominancy of the combustion regime, which is an exothermic process. The maximum temperatures from the LC, RH, and WS feedstocks were observed to be 1478 K, 1034 K, and 1045 K, respectively. Among these, it was also observed that Lakhra coal exhibited the highest temperature compared to the other biomass feedstocks due to the presence of higher fixed carbon in the coal.

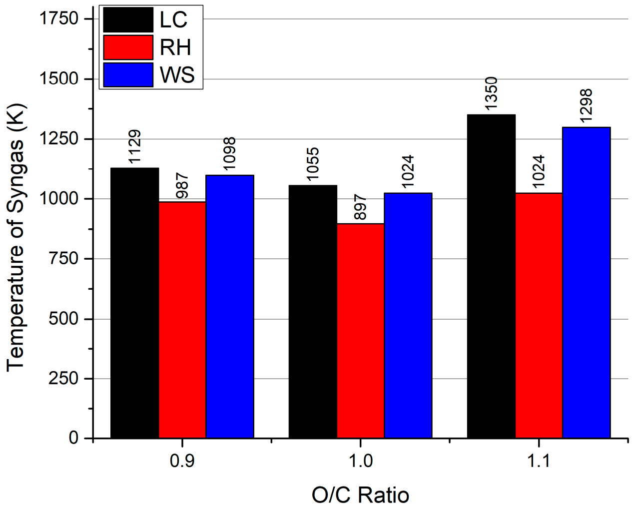

(**a**) Feedstock feeding rate = 0.005 kg/s

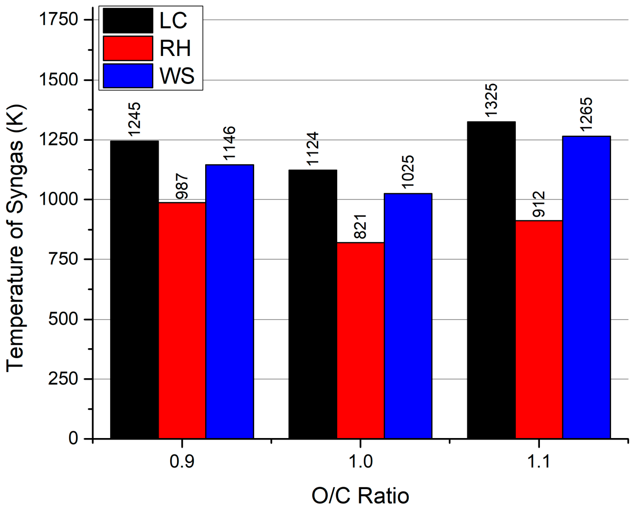

(**b**) Feedstock feeding rate = 0.01 kg/s

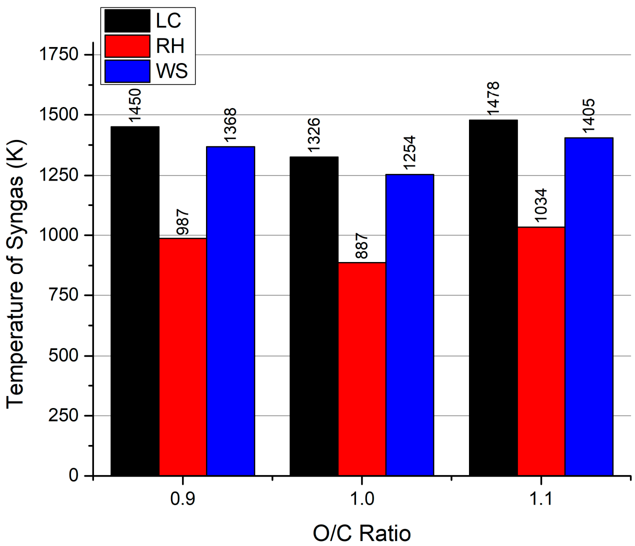

(**c**) Feedstock feeding rate = 0.015 kg/s

Figure 7. Temperature of syngas at varying O/C ratios and feeding rates.

To evaluate the impact of axial and tangential multi-opposite burners in the development of flameless combustion/gasification, the temperature profiles were obtained at both the injection levels (upper and lower) for LC feedstock simulation cases (Figure 8). It was observed that heat was thoroughly mixed for the 1.0 O/C ratio case and the high-temperature zones were homogenized, consistent with previous research [54]. The 1.0 O/C ratio was also considered as the optimized condition for achieving flameless gasification.

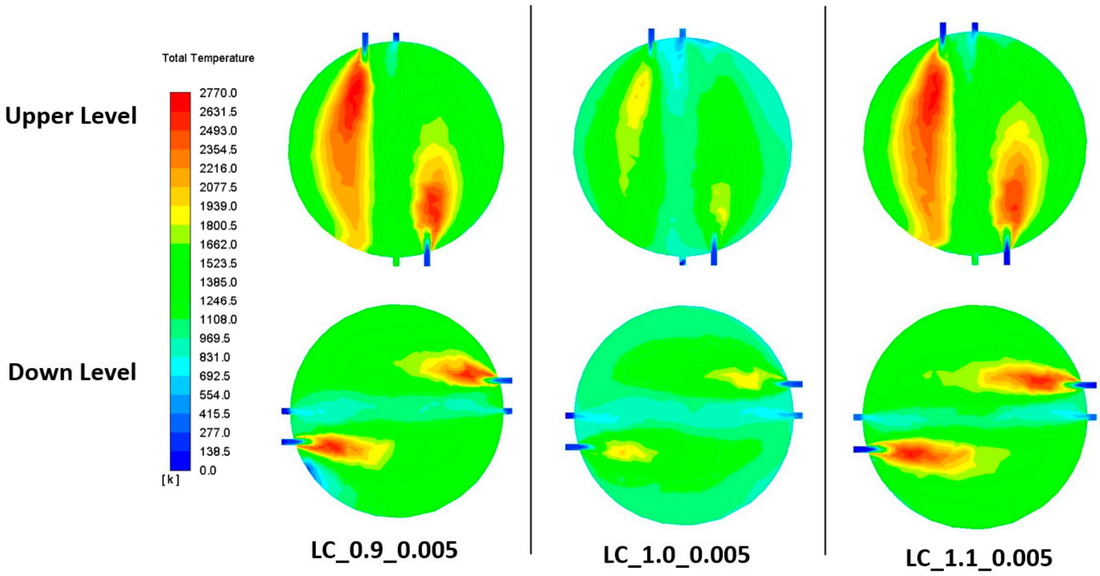

(**a**) Lakhra coal @ 0.005 kg/s feeding rate

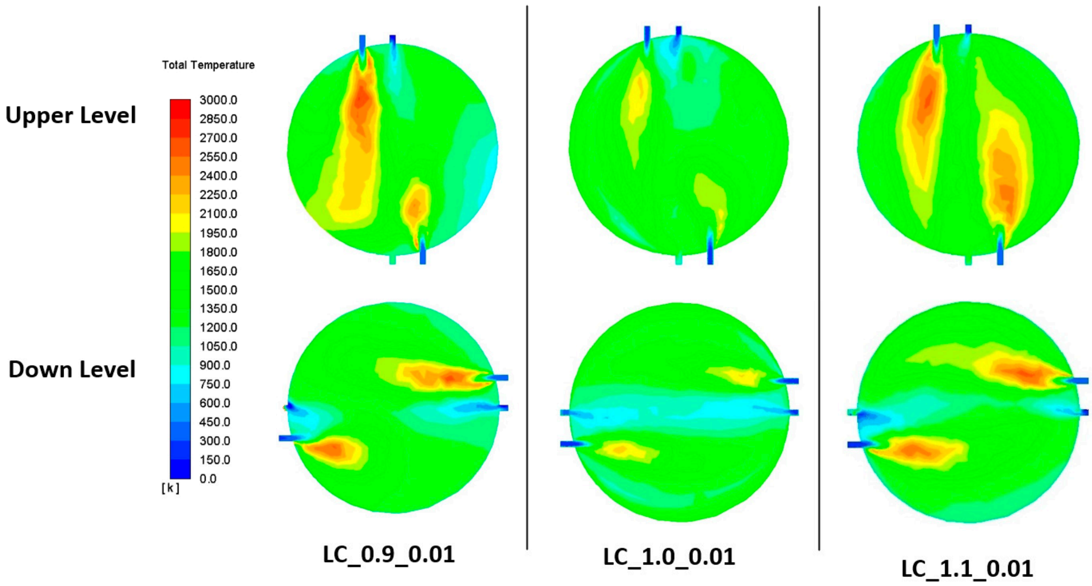

(**b**) Lakhra coal @ 0.01 kg/s feeding rate

Figure 8. *Cont.*

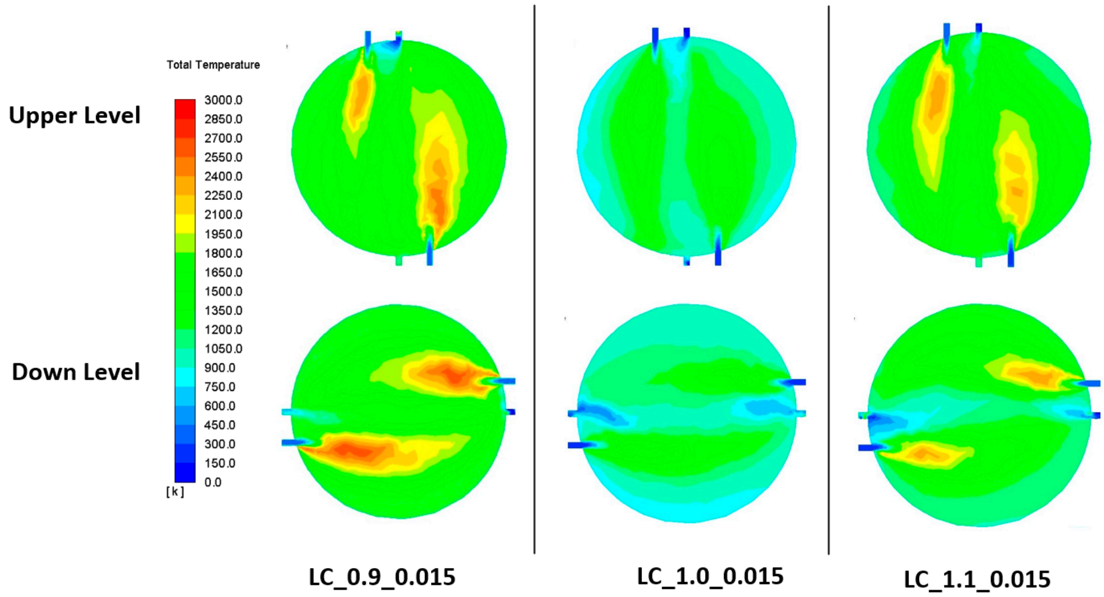

(**c**) Lakhra coal @ 0.015 kg/s feeding rate

Figure 8. Temperature contours for upper and lower injection levels.

3.4. Quality of Produced Syngas

Syngas quality is another important aspect to evaluate the performance of the gasification process. Higher heating value (HHV) is a typical parameter to check the syngas quality, expressing the total heat contents of syngas in terms of combustible substances like CO and H_2. The quality of produced syngas was evaluated by estimating its HHV. The HHV was estimated for all the cases at O/C ratio = 1.0 (as this gave maximum CO and H_2 composition). The HHV was estimated using an Aspen HYSYS V11 simulator through the Peng–Robbinson Fluid Package. Figure 9 illustrates the extracted results for HHV estimation for syngas produced from selected feedstocks at varying feed rates. It was observed that the HHV of syngas was decreased by increasing the feeding rate of feedstock, keeping a constant O/C ratio. The reason for this behavior is a decreasing trend in CO and H_2 production at higher feed rates due to the dominancy of combustion reactions at elevated feed rates, as also explained by previous research [32,48,55]. The maximum HHVs for LC, RH, and WS were estimated as 11,412.47 kJ/kg, 9732.29 kJ/kg, and 8779.2 kJ/kg, respectively.

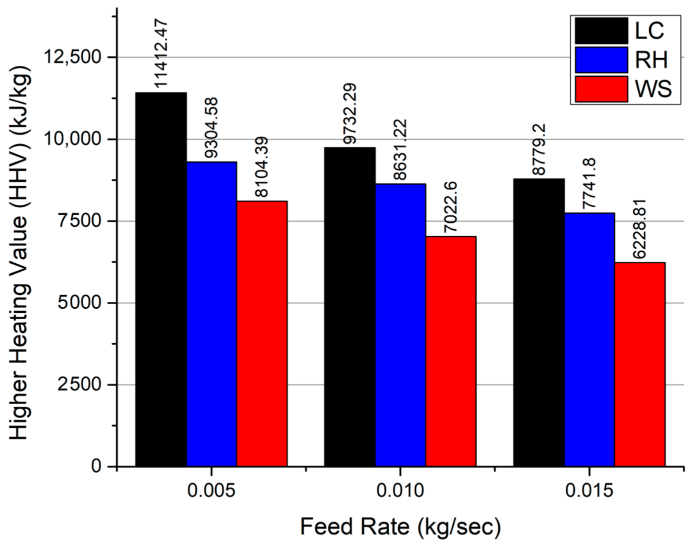

Figure 9. Heating value of syngas produced from selected feedstocks.

3.5. Conversion of Char and Volatiles

Solid feedstocks such as coal or biomasses possess char and volatiles in their composition. Char is the mixture of fixed carbon available in solid fuel with its ash contents, whereas volatiles are hydrocarbons that could be evaporated from coal at higher temperatures. Since volatiles constitute higher hydrocarbons, they can play a crucial role in combustion and contribute significantly in solid fuel combustion/gasification. The conversion of char refers to the consumption of fixed carbon available in the feedstock through heterogeneous reactions (Equations (7)–(9)), whereas the conversion of volatiles refers to the evaporation of volatiles from feedstock (Equation (1)) and their subsequent combustion (Equations (18)–(20)). The char and volatile conversions for all simulated cases are depicted in Figure 10a,b.

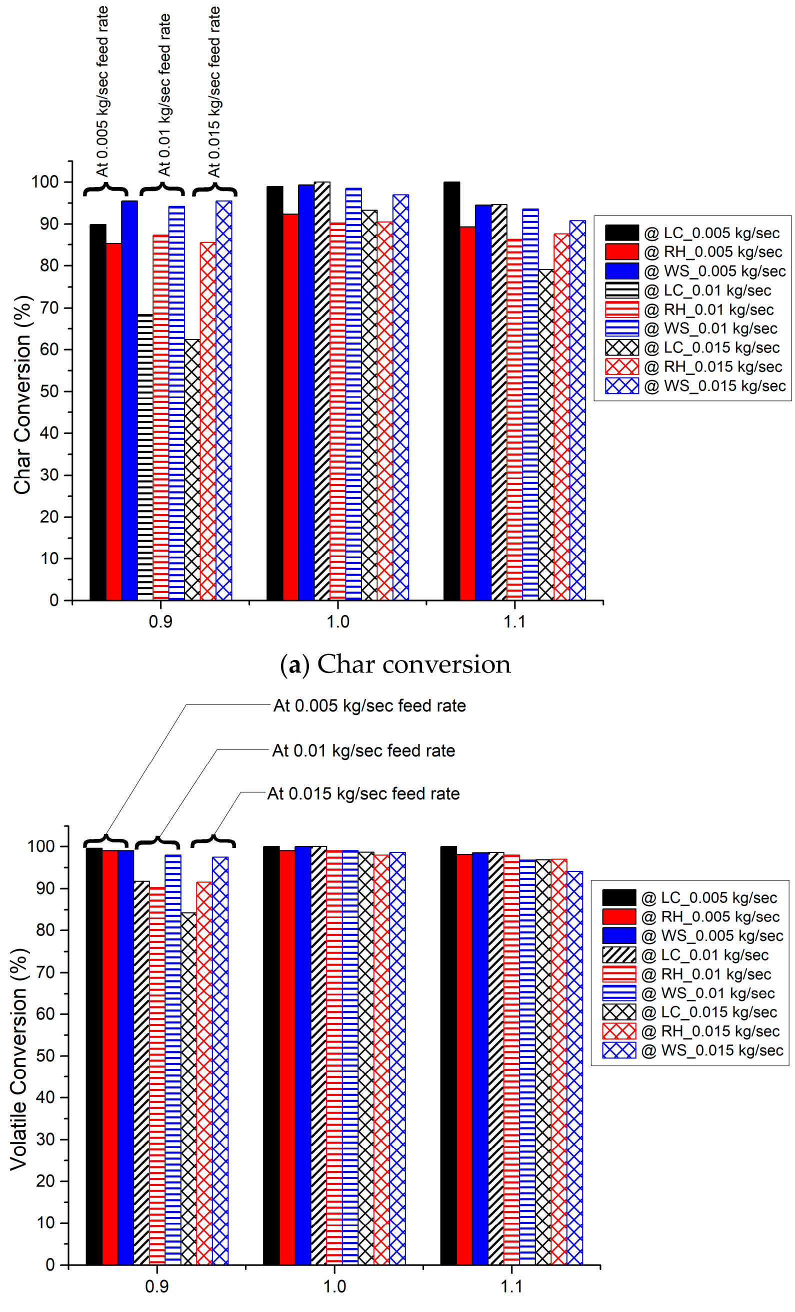

(**a**) Char conversion

(**b**) Volatile conversion

Figure 10. Char and volatile conversions at varying O/C ratios and feeding rates.

It was observed that the maximum char or volatiles conversion was achieved at 1.0 or above O/C ratios in most cases. The maximum char conversions for LC, RH, and WS were observed to be 99.9%, 98.9%, and 99.3%, respectively, at a 0.005 kg/s feed rate. The maximum volatiles conversion for LC, RH, and WS were observed to be 100%, 99%, and 100%, respectively, at the same feeding rate. Similarly, with increased feedstock flowrate (0.01 kg/s), it was again observed that the maximum char or volatiles conversion achieved was at the 1.0 O/C ratios for all the case results. The maximum char conversions at the 0.01 kg/s feeding rate for LC, RH, and WS were observed to be 99.9%, 90.24%, and 98.5%, respectively. The maximum volatiles conversion for LC, RH, and WS were observed to be 100%, 99%, and 99%, respectively, at the same feeding rate.

It was observed that at a higher feed flowrate (0.015 kg/s), the overall conversion of char or volatile decreased. The maximum char conversions for LC, RH, and WS were observed to be 93.26%, 90.54%, and 97%, respectively, at the 10 O/C ratio. The maximum volatiles conversion for LC, RH, and WS were observed to be 98.65%, 98%, and 98.6%, respectively. These findings confirm the trends of char or volatile conversion from previous studies [45,46].

3.6. Conversion Efficiencies

The overall performance of a gasifier can be evaluated via its carbon conversion efficiency (CCE) and cold conversion efficiency (CGE). The carbon conversion efficiency shows the conversion of fixed carbon into CO and CO_2, whereas the cold conversion efficiency expresses the conversion of fixed carbon into CO and H_2. Both the CCE and CGE were estimated using Equations (21) and (22), respectively. Figure 11 presents the efficiencies for coal and biomass samples at the 1.0 O/C ratio. It was observed that the CCE for all the feedstocks was above 90% at the investigated feeding rates. This shows the high performance of the gasification system and also confirms the char conversion data of the previous section. The highest CCE was observed in the range of 98% for WS due to higher amounts of CO_2 production from this particular feedstock. Conversely, the CGE was higher at low feeding rates and decreased with increasing feeding rate. The maximum CGE was observed for LC 92.9% at 0.005 kg/s, whereas the most minimum CGE was observed for WS 59.57% at a 0.015 kg/s feeding rate.

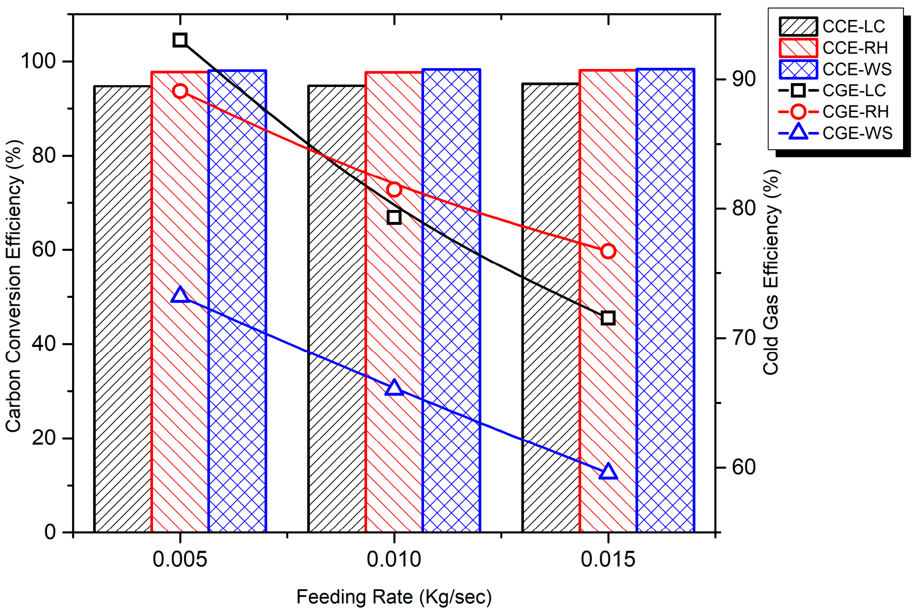

Figure 11. Carbon conversion efficiency and cold gas efficiency for selected feedstock at 1.0 O/C ratio.

3.7. Flow Visualization

The multi-opposite burner (MOB) gasifier is a special type of entrained flow gasification configuration in which the vortex in the flow is created with multi-opposite injectors. In such devices, the flow behavior plays an important role due to the recirculation of exhaust gases for creating a flameless scenario. For the understanding and visualization the flow behavior, three cases of coal were selected with 0.005, 0.01, and 0.015 kg/s coal feeding rates at 1.0 O/C ratios. The flow streamlines with velocity are shown in Figure 12. It was observed that reduced feeding rates, corresponding to lower mass flowrates of oxidants, result in significant differences in both velocity profiles and flow behavior. A strong vortex formation can be seen with the high feeding rate case, i.e., 0.015 kg/s.

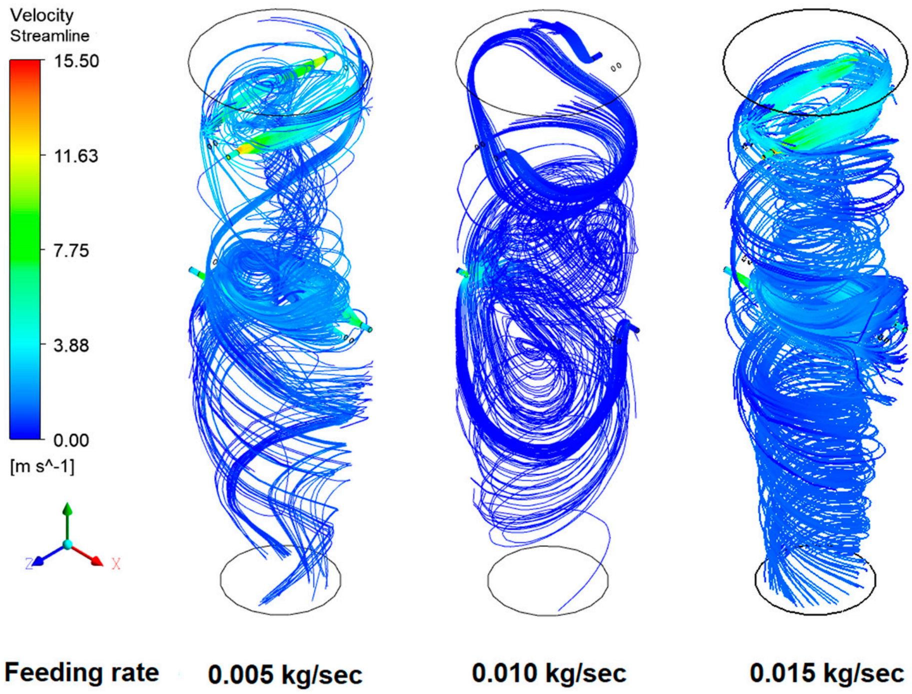

Figure 12. Flow streamlines with velocity as variable for LC cases with 1.0 O/C ratio.

3.8. Comparison of Simulated Results with Published Work

The present simulated results of the CO, CO_2, and H_2 mole fraction of syngas were compared with those reported in previously published work [29,41,45,53–60] as depicted in Figure 13. It can be seen that results of most of the literature are closer, apart from a few exceptional cases. A more rigorous comparison can be performed with the RH and SW cases presented by Maitlo, Unar [45], in which CO is in closer ranges. However, CO_2 is a little lower and H_2 is a little higher for the current study, which could be due to the use of different technology. In these studies, a concentric tube gasifier was used, which is different from the presently modeled MOB gasifier, which is based on a flameless strategy.

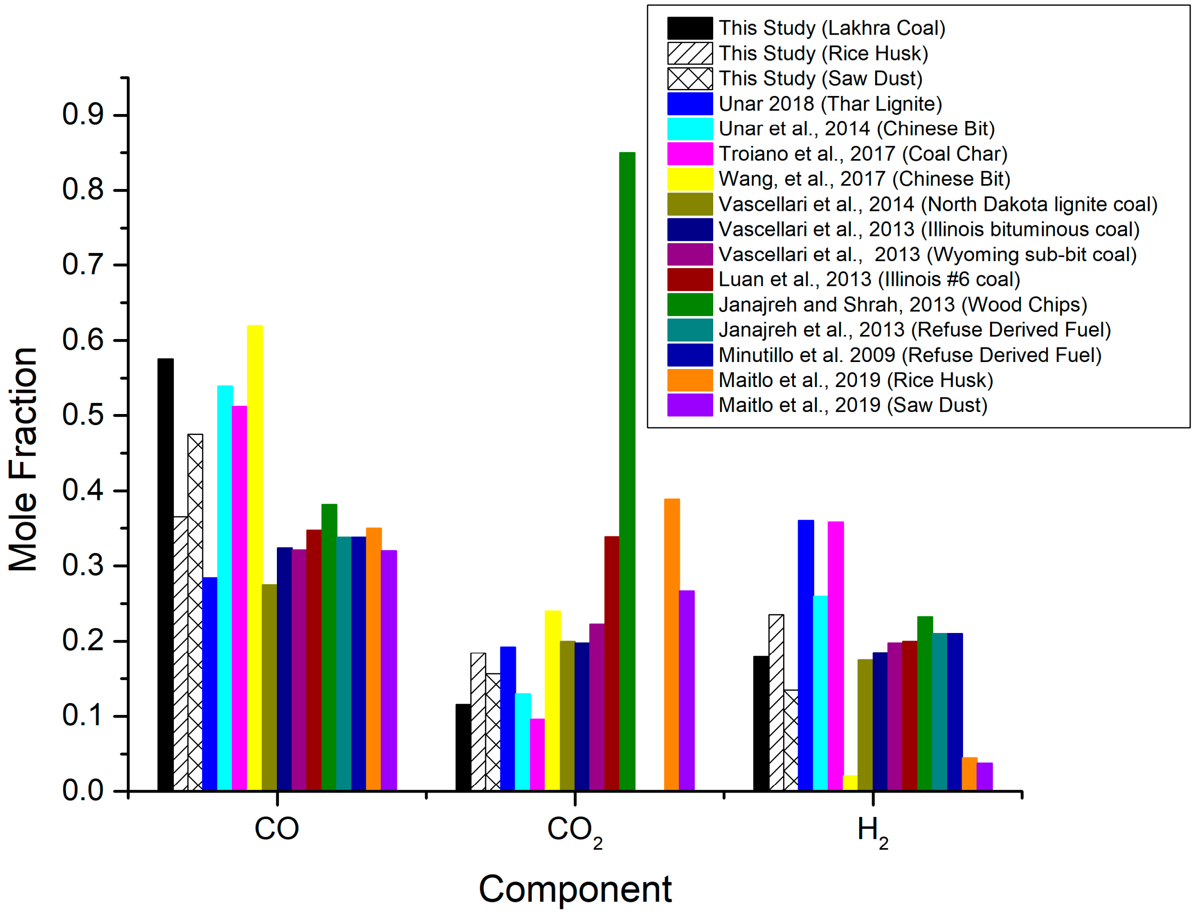

Figure 13. Comparison of simulated mole fractions of CO, CO_2, and H_2 in syngas with published literature [32,44,48,56–63].

4. Conclusions

A 3D CFD model for a multi-opposite burner gasifier was successfully developed and validated with published research against the syngas composition. Among the different reaction schemes, scheme E (which involves complete volatile and char combustion reactions) produced better results based on comparative analysis with previously published results. Hence, scheme E was validated and subsequently used for the rest of simulation study. It is concluded that a O/C ratio 1.0 gives better results in terms of the composition of CO and H_2 in produced syngas. The feed rate exhibited an inverse relationship with the overall gasifier performance. Increasing the feed rate decreased the CO and H_2 composition in the syngas.

The maximum CO and H_2 percentages were 57.59% and 16.58%, respectively, for Lakhra coal at a 1.0 O/C ratio and 0.005 kg/s feed rate. Rice husk achieved maximum CO and H_2 percentages of 36.57% and 23.54%, while sawdust reached 47.54% and 13.47% under the same conditions. The syngas exit temperatures were highest for Lakhra coal at 1478 K, compared to 1034 K and 1045 K for rice husk and sawdust. The temperature profiles indicate that the impinging and tangential nozzles favored gasification at a 1.0 O/C ratio, resulting in a flameless scenario. The flow streams show the development of a strong vortex due to impinging and tangential multi-opposite injectors.

The char conversion rates were notably high, with 99% for Lakhra coal, 98.9% for rice husk, and 99.3% for sawdust. Volatile conversion ranged from 94% to 100% for all feedstocks. The higher heating value (HHV) of syngas decreased with increasing feed rate. The maximum HHVs were 11,412.47 kJ/kg for Lakhra coal, 9732.29 kJ/kg for rice husk, and 8779.2 kJ/kg for sawdust. Comparing the syngas composition with the literature, the CO predictions were slightly higher, while CO_2 and H_2 were generally within similar ranges, with a few exceptions.

Author Contributions: Conceptualization, I.N.U., M.A. and K.Q.; methodology, A.u.R.; software, A.u.R. and S.A.; validation, A.u.R.; formal analysis, I.N.U. and S.A.; investigation, A.u.R.; resources, K.Q. and A.S.J.; data curation, S.A.; writing—original draft preparation, A.u.R.; writing—review and editing, A.S.J.; supervision, I.N.U., M.A. and K.Q.; funding acquisition, A.S.J. All authors have read and agreed to the published version of the manuscript.

Funding: This research received no external funding.

Data Availability Statement: Data available on request due to restrictions, e.g., privacy or ethical. The data presented in this study are available on request from the corresponding author. The data are not publicly available due to ongoing research projects.

Acknowledgments: The authors are thankful to Mehran University of Engineering and Technology, Jamshoro, Pakistan for providing valuable resources and support in the accomplishment of this research article.

Conflicts of Interest: The authors declare no conflict of interest.

References

1. Akaev, A.; Davydova, O. Climate and Energy: Energy Transition Scenarios and Global Temperature Changes Based on Current Technologies and Trends. In *Reconsidering the Limits to Growth: A Report to the Russian Association of the Club of Rome*; Springer: Cham, Switzerland, 2023; pp. 53–70.
2. Zhan, X.; Zhou, Z.; Wang, F. Catalytic effect of black liquor on the gasification reactivity of petroleum coke. *Appl. Energy* **2010**, *87*, 1710–1715. [CrossRef]
3. Jakobs, T.; Djordjevic, N.; Fleck, S.; Mancini, M.; Weber, R.; Kolb, T. Gasification of high viscous slurry R&D on atomization and numerical simulation. *Appl. Energy* **2012**, *93*, 449–456.
4. Shen, C.-H.; Chen, W.-H.; Hsu, H.-W.; Sheu, J.-Y.; Hsieh, T.-H. Co-gasification performance of coal and petroleum coke blends in a pilot-scale pressurized entrained-flow gasifier. *Int. J. Energy Res.* **2012**, *36*, 499–508. [CrossRef]
5. McKendry, P. Energy production from biomass (part 1): Overview of biomass. *Bioresour. Technol.* **2002**, *83*, 37–46. [CrossRef] [PubMed]
6. Umeki, K.; Namioka, T.; Yoshikawa, K. Analysis of an updraft biomass gasifier with high temperature steam using a numerical model. *Appl. Energy* **2012**, *90*, 38–45. [CrossRef]
7. Gani, A.; Zaki, M.; Mamat, R.; Nizar, M.; Rosdi, S.; Yana, S.; Sarjono, R. Analysis of technological developments and potential of biomass gasification as a viable industrial process: A review. *Case Stud. Chem. Environ. Eng.* **2023**, *8*, 100439.
8. Chmielniak, T.; Sciazko, M. Co-gasification of biomass and coal for methanol synthesis. *Appl. Energy* **2003**, *74*, 393–403. [CrossRef]
9. Chen, W.-H.; Wu, J.-S. An evaluation on rice husks and pulverized coal blends using a drop tube furnace and a thermogravimetric analyzer for application to a blast furnace. *Energy* **2009**, *34*, 1458–1466. [CrossRef]
10. Ma, M.; Bai, Y.; Wei, J.; Song, X.; Lv, P.; Wang, J.; Su, W.; Xiong, Q.; Yu, G. Decoupling study of volatile–char interaction during coal/biomass co-gasification based on a two-stage fixed bed reactor: Insight into the role of O-containing compound species. *Chem. Eng. Sci.* **2023**, *265*, 118262. [CrossRef]
11. Chen, W.-H.; Chen, J.-C.; Tsai, C.-D.; Jiang, T.L. Transient gasification and syngas formation from coal particles in a fixed-bed reactor. *Int. J. Energy Res.* **2007**, *31*, 895–911. [CrossRef]
12. Pettinau, A.; Ferrara, F.; Amorino, C. Techno-economic comparison between different technologies for a CCS power generation plant integrated with a sub-bituminous coal mine in Italy. *Appl. Energy* **2012**, *99*, 32–39. [CrossRef]
13. McKendry, P. Energy production from biomass (part 2): Conversion technologies. *Bioresour. Technol.* **2002**, *83*, 47–54. [CrossRef] [PubMed]
14. Srirangan, K.; Akawi, L.; Moo-Young, M.; Chou, C.P. Towards sustainable production of clean energy carriers from biomass resources. *Appl. Energy* **2012**, *100*, 172–186. [CrossRef]
15. Pereira, E.G.; da Silva, J.N.; de Oliveira, J.L.; Machado, C.S. Sustainable energy: A review of gasification technologies. *Renew. Sustain. Energy Rev.* **2012**, *16*, 4753–4762. [CrossRef]
16. Dhrioua, M.; Ghachem, K.; Hassen, W.; Ghazy, A.; Kolsi, L.; Borjini, M.N. Simulation of biomass air gasification in a bubbling fluidized bed using aspen plus: A comprehensive model including tar production. *ACS Omega* **2022**, *7*, 33518–33529. [CrossRef] [PubMed]
17. Guo, F.; Dong, Y.; Dong, L.; Guo, C. Effect of design and operating parameters on the gasification process of biomass in a downdraft fixed bed: An experimental study. *Int. J. Hydrogen Energy* **2014**, *39*, 5625–5633. [CrossRef]
18. Chen, C.; Horio, M.; Kojima, T. Use of numerical modeling in the design and scale-up of entrained flow coal gasifiers. *Fuel* **2001**, *80*, 1513–1523. [CrossRef]

19. Slezak, A.; Kuhlman, J.M.; Shadle, L.J.; Spenik, J.; Shi, S. CFD simulation of entrained-flow coal gasification: Coal particle density/sizefraction effects. *Powder Technol.* **2010**, *203*, 98–108. [CrossRef]
20. Wu, Y.X.; Zhang, J.S.; Yue, G.X.; Lü, J.F. Analysis of the Gasification Performance of a Staged Entrained Flow Gasifier by Presumed PDF Model. *Proc. CSEE* **2008**, *26*, 007.
21. Andries, J.; Becht, J.; Hoppesteyn, P. Pressurized fluidized bed combustion and gasification of coal using flue gas recirculation and oxygen injection. *Energy Convers. Manag.* **1997**, *38*, S117–S122. [CrossRef]
22. Nguyen, T.D.; Ngo, S.I.; Lim, Y.-I.; Lee, J.W.; Lee, U.-D.; Song, B.-H. Three-stage steady-state model for biomass gasification in a dual circulating fluidized-bed. *Energy Convers. Manag.* **2012**, *54*, 100–112. [CrossRef]
23. Vicente, W.; Ochoa, S.; Aguillón, J.; Barrios, E. An Eulerian model for the simulation of an entrained flow coal gasifier. *Appl. Therm. Eng.* **2003**, *23*, 1993–2008. [CrossRef]
24. Gerun, L.; Paraschiv, M.; Vîjeu, R.; Bellettre, J.; Tazerout, M.; Gøbel, B.; Henriksen, U. Numerical investigation of the partial oxidation in a two-stage downdraft gasifier. *Fuel* **2008**, *87*, 1383–1393. [CrossRef]
25. Álvarez, L.; Gharebaghi, M.; Jones, J.; Pourkashanian, M.; Williams, A.; Riaza, J.; Pevida, C.; Pis, J.; Rubiera, F. Numerical investigation of NO emissions from an entrained flow reactor under oxy-coal conditions. *Fuel Process. Technol.* **2012**, *93*, 53–64. [CrossRef]
26. Fletcher, D.; Haynes, B.; Christo, F.; Joseph, S. A CFD based combustion model of an entrained flow biomass gasifier. *Appl. Math. Model.* **2000**, *24*, 165–182. [CrossRef]
27. Ajilkumar, A.; Sundararajan, T.; Shet, U.S.P. Numerical modeling of a steam-assisted tubular coal gasifier. *Int. J. Therm. Sci.* **2009**, *48*, 308–321. [CrossRef]
28. Chui, E.; Majeski, A.; Lu, D.; Hughes, R.; Gao, H.; McCalden, D.; Anthony, E. Simulation of entrained flow coal gasification. *Energy Procedia* **2009**, *1*, 503–509. [CrossRef]
29. Dong, C.; Yang, Y.; Yang, R.; Zhang, J. Numerical modeling of the gasification based biomass co-firing in a 600 MW pulverized coal boiler. *Appl. Energy* **2010**, *87*, 2834–2838. [CrossRef]
30. Chen, C.-J.; Hung, C.-I.; Chen, W.-H. Numerical investigation on performance of coal gasification under various injection patterns in an entrained flow gasifier. *Appl. Energy* **2012**, *100*, 218–228. [CrossRef]
31. Zheng, L.; Furinsky, E. Comparison of Shell, Texaco, BGL and KRW gasifiers as part of IGCC plant computer simulations. *Energy Convers. Manag.* **2005**, *46*, 1767–1779. [CrossRef]
32. Unar, I.N.; Wang, L.; Pathan, A.G.; Mahar, R.B.; Li, R.; Uqaili, M.A. Numerical simulations for the coal/oxidant distribution effects between two-stages for multi opposite burners (MOB) gasifier. *Energy Convers. Manag.* **2014**, *86*, 670–682. [CrossRef]
33. Li, C.; Dai, Z.; Li, W.; Xu, J.; Wang, F. 3D numerical study of particle flow behavior in the impinging zone of an Opposed Multi-Burner gasifier. *Powder Technol.* **2012**, *225*, 118–123. [CrossRef]
34. Ni, J.; Liang, Q.; Zhou, Z.; Dai, Z.; Yu, G. Numerical and experimental investigations on gas–particle flow behaviors of the Opposed Multi-Burner Gasifier. *Energy Convers. Manag.* **2009**, *50*, 3035–3044. [CrossRef]
35. Masmoudi, M.A.; Sahraoui, M.; Grioui, N.; Halouani, K. 2-D Modeling of thermo-kinetics coupled with heat and mass transfer in the reduction zone of a fixed bed downdraft biomass gasifier. *Renew. Energy* **2014**, *66*, 288–298. [CrossRef]
36. Mahmoudi, A.H.; Hoffmann, F.; Peters, B. Application of XDEM as a novel approach to predict drying of a packed bed. *Int. J. Therm. Sci.* **2014**, *75*, 65–75. [CrossRef]
37. Cau, G.; Tola, V.; Pettinau, A. A steady state model for predicting performance of small-scale up-draft coal gasifiers. *Fuel* **2015**, *152*, 3–12. [CrossRef]
38. Patel, K.D.; Shah, N.K.; Patel, R.N. CFD Analysis of Spatial Distribution of Various Parameters in Downdraft Gasifier. *Procedia Eng.* **2013**, *51*, 764–769. [CrossRef]
39. Murgia, S.; Vascellari, M.; Cau, G. Comprehensive CFD model of an air-blown coal-fired updraft gasifier. *Fuel* **2012**, *101*, 129–138. [CrossRef]
40. Wu, Y.; Zhang, Q.; Yang, W.; Blasiak, W. Two-dimensional computational fluid dynamics simulation of biomass gasification in a downdraft fixed-bed gasifier with highly preheated air and steam. *Energy Fuels* **2013**, *27*, 3274–3282. [CrossRef]
41. Ambatipudi, M.K.; Varunkumar, S. A novel MILD gasifier for crushed low-grade solid fuels. *Proc. Combust. Inst.* **2023**, *39*, 3479–3488. [CrossRef]
42. Dhrioua, M.; Hassen, W.; Kolsi, L.; Anbumalar, V.; Alsagri, A.S.; Borjini, M.N. Gas distributor and bed material effects in a cold flow model of a novel multi-stage biomass gasifier. *Biomass Bioenergy* **2019**, *126*, 14–25. [CrossRef]
43. Zhang, Z.; Lu, B.; Zhao, Z.; Zhang, L.; Chen, Y.; Li, S.; Luo, C.; Zheng, C. CFD modeling on char surface reaction behavior of pulverized coal MILD-oxy combustion: Effects of oxygen and steam. *Fuel Process. Technol.* **2020**, *204*, 106405. [CrossRef]
44. Wang, L.; Jia, Y.; Kumar, S.; Li, R.; Mahar, R.B.; Ali, M.; Unar, I.N.; Sultan, U.; Memon, K. Numerical analysis on the influential factors of coal gasification performance in two-stage entrained flow gasifier. *Appl. Therm. Eng.* **2017**, *112*, 1601–1611. [CrossRef]
45. Wen, C.; Chaung, T. Entrainment coal gasification modeling. *Ind. Eng. Chem. Process Des. Dev.* **1979**, *18*, 684–695. [CrossRef]
46. Du, S.-W.; Chen, W.-H.; Lucas, J. Performances of pulverized coal injection in blowpipe and tuyere at various operational conditions. *Energy Convers. Manag.* **2007**, *48*, 2069–2076. [CrossRef]
47. Du, S.-W.; Chen, W.-H. Numerical prediction and practical improvement of pulverized coal combustion in blast furnace. *Int. Commun. Heat Mass Transf.* **2006**, *33*, 327–334. [CrossRef]

48. Maitlo, G.; Unar, I.N.; Mahar, R.B.; Brohi, K.M. Numerical simulation of lignocellulosic biomass gasification in concentric tube entrained flow gasifier through computational fluid dynamics. *Energy Explor. Exploit.* **2019**, *37*, 1073–1097. [CrossRef]
49. Unar, I.N.; Soomro, S.A.; Maitlo, G.; Aziz, S.; Mahar, R.B.; Bhatti, Z.A. Numerical study of coal composition effects on the performance of gasification through computational fluid dynamic. *Int. J. Chem. React. Eng.* **2019**, *17*, 20180204. [CrossRef]
50. Zhang, Z.; Lu, B.; Zhao, Z.; Zhang, L.; Chen, Y.; Luo, C.; Zheng, C. Heterogeneous reactions behaviors of pulverized coal MILD combustion under different injection conditions. *Fuel* **2020**, *275*, 117925. [CrossRef]
51. Skodras, G.; Someus, E.; Grammelis, P.; Palladas, A.; Amarantos, P.; Basinas, P.; Natas, P.; Prokopidou, M.; Diamantopoulou, I.; Kakaras, E.; et al. Combustion and environmental performance of clean coal end products. *Int. J. Energy Res.* **2007**, *31*, 1237. [CrossRef]
52. Macías-García, A.; Cuerda-Correa, E.M.; Díaz-Díez, M.A. Application of the Rosin–Rammler and Gates–Gaudin–Schuhmann models to the particle size distribution analysis of agglomerated cork. *Mater. Charact.* **2004**, *52*, 159–164. [CrossRef]
53. Maitlo, G.; Ali, I.; Mangi, K.H.; Ali, S.; Maitlo, H.A.; Unar, I.N.; Pirzada, A.M. Thermochemical conversion of biomass for syngas production: Current status and future trends. *Sustainability* **2022**, *14*, 2596. [CrossRef]
54. Chanphavong, L.; Al-Attab, K.; Zainal, Z.A. Flameless Combustion Characteristics of Producer Gas Premixed Charge in a Cyclone Combustor. *Flow Turbul. Combust.* **2019**, *103*, 731–750. [CrossRef]
55. Rauch, R.; Hrbek, J.; Hofbauer, H. Biomass gasification for synthesis gas production and applications of the syngas. *Wiley Interdiscip. Rev. Energy Environ.* **2014**, *3*, 343–362. [CrossRef]
56. Minutillo, M.; Perna, A.; Di Bona, D. Modelling and performance analysis of an integrated plasma gasification combined cycle (IPGCC) power plant. *Energy Convers. Manag.* **2009**, *50*, 2837–2842. [CrossRef]
57. Janajreh, I.; Al Shrah, M. Numerical and experimental investigation of downdraft gasification of wood chips. *Energy Convers. Manag.* **2013**, *65*, 783–792. [CrossRef]
58. Janajreh, I.; Raza, S.S.; Valmundsson, A.S. Plasma gasification process: Modeling, simulation and comparison with conventional air gasification. *Energy Convers. Manag.* **2013**, *65*, 801–809. [CrossRef]
59. Luan, Y.-T.; Chyou, Y.-P.; Wang, T. Numerical analysis of gasification performance via finite-rate model in a cross-type two-stage gasifier. *Int. J. Heat Mass Transf.* **2013**, *57*, 558–566. [CrossRef]
60. Vascellari, M.; Arora, R.; Pollack, M.; Hasse, C. Simulation of entrained flow gasification with advanced coal conversion submodels. Part 1: Pyrolysis. *Fuel* **2013**, *113*, 654–669. [CrossRef]
61. Vascellari, M.; Arora, R.; Hasse, C. Simulation of entrained flow gasification with advanced coal conversion submodels. Part 2: Char conversion. *Fuel* **2014**, *118*, 369–384. [CrossRef]
62. Troiano, M.; Santagata, T.; Montagnaro, F.; Salation, P. Impact experiments of char and ash particles relevant to entrained-flow coal gasifiers. *Fuel* **2017**, *202*, 665–674. [CrossRef]
63. Unar, I.N. Kinetic Modeling of Gasification Reactions for Lignite Coal Under High Pressure. Ph.D. Thesis, Mehran University of Engineering & Technology, Jamshoro, Pakistan, 2018.

Disclaimer/Publisher's Note: The statements, opinions and data contained in all publications are solely those of the individual author(s) and contributor(s) and not of MDPI and/or the editor(s). MDPI and/or the editor(s) disclaim responsibility for any injury to people or property resulting from any ideas, methods, instructions or products referred to in the content.